Behavioral/Systems/Cognitive

Light-Evoked Excitatory and Inhibitory Synaptic Inputs to ON and OFF α Ganglion Cells in the Mouse Retina

Ji-Jie Pang, Fan Gao, and Samuel M. Wu
Cullen Eye Institute, Baylor College of Medicine, Houston, Texas 77030

Bipolar cell and amacrine cell synaptic inputs to α ganglion cells (αGCs) in dark-adapted mouse retinas were studied by recording the light-evoked excitatory cation current (ΔI_C) and inhibitory chloride current (ΔI_{Cl}) under voltage-clamp conditions, and the cell morphology was revealed by Lucifer yellow fluorescence with a confocal microscope. Three types of αGCs were identified. (1) ONαGCs exhibits no spike activity in darkness, increased spikes in light, sustained inward ΔI_C, sustained outward ΔI_{Cl} of varying amplitude, and large soma (20–25 μm in diameter) with α-cell-like dendritic field ~180–350 μm stratifying near 70% of the inner plexiform layer (IPL) depth. (2) Transient OFFαGCs (tOFFαGCs) exhibit no spike activity in darkness, transient increased spikes at light offset, small sustained outward ΔI_C in light, a large transient inward ΔI_C at light offset, a sustained outward ΔI_{Cl}, and a morphology similar to the ONαGCs except for that their dendrites stratified near 30% of the IPL depth. (3) Sustained OFFαGCs exhibit maintained spike activity of 5–10 Hz in darkness, sustained decrease of spikes in light, sustained outward ΔI_C, sustained outward ΔI_{Cl}, and a morphology similar to the tOFFαGCs. By comparing the response thresholds and dynamic ranges of αGCs with those of the preganglion cells, our data suggest that the light responses of each type of αGCs are mediated by different sets of bipolar cells and amacrine cells. This detailed physiological analysis complements the existing anatomical results and provides new insights on the functional roles of individual synapses in the inner mammalian retina.

Key words: **α ganglion cells; light responses; rod bipolar cells; M-cone bipolar cells; S-cone bipolar cells; AII amacrine cells; response threshold; dynamic range**

Introduction

Parallel information processing is a fundamental principle for sensory signal encoding in the brain, and two of the most important and well described signaling pathways in the visual system are the ON and OFF channels (Hubel and Wiesel, 1968). Anatomical studies during the past 30 years have suggested that the ON and OFF synaptic pathways in all mammal retinas follow the same plan: cones make synapses on cone depolarizing (ON) and hyperpolarizing (OFF) bipolar cells (DBC_Cs and HBC_Cs), which synapse on the ON and OFF ganglion cells, respectively (Kolb and Famiglietti, 1974; Nelson et al., 1978, 1981). Rods make synaptic contacts with only one type of bipolar cell that depolarizes in response to light spots (DBC_R). DBC_Rs synapse on the AII amacrine cells that make electrical synapses with DBC_Cs and inhibitory chemical synapses (probably glycinergic) with HBC_Cs and OFF ganglion cells (Bolz et al., 1984; Pourcho and Owczarzak, 1991; Crooks and Kolb, 1992). According to this plan, HBCs do not receive inputs directly from rods, and ON and OFF ganglion cells do not receive inputs directly from rod bipolar cells but by the DBC_R–AII pathway (Kolb and Nelson, 1981, 1983; Wassle and Boycott, 1991). Evidence from recent studies, however, begins to challenge this view. In the rabbit retina, for example, when rod–DBC_R synapses are blocked by APB, rod inputs to OFF ganglion cells persist, indicative of an alternative rod–OFF ganglion cell synaptic pathway (DeVries and Baylor, 1995). Studies on normal and coneless transgenic mice indicate that rods make synaptic inputs directly to HBCs (Soucy et al., 1998; Tsukamoto et al., 2001). These results suggest that the physiological responses of ON and OFF ganglion cells in mammalian retinas may be mediated by a synaptic network more complex than the general plan set forth by previous anatomical studies. Additionally, it is not clear whether all anatomically identified synapses made on ganglion cells are functional and how effective each of the bipolar cell and amacrine cell synapses transfers light-evoked signals. Systematic physiological analysis of the synaptic inputs mediating light-evoked excitatory and inhibitory responses of ON and OFF ganglion cells is needed to resolve these outstanding questions.

Most ganglion cell light responses in mammalian retina have been recorded by single or arrays of extracellular electrodes (Kuffler, 1953; Meister et al., 1991). The advantage of these techniques is that they allow stable recordings for long periods of time with minimum electrode damage to the cells. The disadvantages of this approach, however, include the inability to measure the transmembrane potential, inability to separate the various synaptic components of light responses, and the inability to inject intracellular dyes to reveal the cell morphology. In this study, we used the whole-cell voltage-clamp technique to record light-

Received March 17, 2003; revised April 29, 2003; accepted May 1, 2003.

This work was supported by National Institutes of Health Grant EY 04446, National Institutes of Health Vision Core Grant EY 02520, the Retina Research Foundation (Houston, TX), and Research to Prevent Blindness. We thank Drs. Laura Frishman, Helga Kolb, Susan Cushman, and Roy Jacoby for critically reading this manuscript.

Correspondence should be addressed to Dr. Samuel M. Wu, Cullen Eye Institute, Baylor College of Medicine, One Baylor Plaza, NC-205, Houston, TX 77030. E-mail: swu@bcm.tmc.edu.

 0270-6474/03/236063-11$15.00/0

evoked responses from the ON and OFF α ganglion cells in the dark-adapted flat-mount mouse retina. We chose the mouse retina because physiological results obtained in wild-type mice can later be correlated with findings in genetically manipulated mice. We chose α ganglion cells (αGCs) because they can be clearly distinguished from other ganglion cells by their distinct morphological signature (Sun et al., 2002), and their large somas are suitable for stable patch-clamp recordings. Moreover, the cellular and synaptic inputs to these cells have been well characterized at the ultrastructural level (Freed and Sterling, 1988; Vardi et al., 1989), and thus physiological findings can be readily correlated with anatomical observations.

Materials and Methods

Experimental approach. Our study constitutes the first voltage-clamp analysis of ganglion cell light responses in the mouse retina, and the major advantage of this approach is that excitatory and inhibitory current responses can be separated by holding the membrane potential near chloride and cation reversal potentials, respectively. Thus, the bipolar cell and amacrine cell contributions to the light responses of the ganglion cells (i.e., cation and chloride currents, or ΔI_C and ΔI_{Cl}, respectively) can be differentially recorded. Because mouse rods are ~2–4 log units more sensitive to green light than cones (Lyubarsky et al., 1999), we use the response threshold to 500 nm lights to estimate the relative rod–cone contributions to ΔI_C and ΔI_{Cl} in each α ganglion cell and thereby determine whether the light responses of the cell are driven by rod- or cone-dominated bipolar–amacrine cells. Another advantage of this approach is that the three-dimensional morphology of the cell can be easily revealed by Lucifer yellow filling with the recording electrode (assisted by a confocal microscope). This allows us to characterize the morphology of each recorded cell and to compare it with results of previous anatomical studies. It also allows us to exclude other types of ganglion cells and displaced amacrine cells [the latter accounts for ~60% of the somas in the mouse ganglion cell layer (Williams et al., 1996; Jeon et al., 1998) and can be easily recognized by the lack of axons]. Additionally, spontaneous and light-evoked spike activities can be conveniently recorded with the patch electrodes in the "loose-patch" mode, permitting us to compare voltage-clamp current responses with the physiological responses of the unclamped cells.

Preparations and light stimulation. The mouse strain used in this study was C57BL/6J from The Jackson Laboratory (Bar Harbor, ME). All animals were handled in accordance with the policies on the treatment of laboratory animals of Baylor College of Medicine. Mice were dark adapted for 1–2 hr before the experiment. To maintain the retina in the fully dark-adapted state, all additional procedures were performed under infrared illumination with dual-unit Nitemare (BE Meyers, Redmond, WA) infrared scopes. Animals were killed by a lethal injection of ketamine plus xylazine plus acepromazine (0.1 ml, 100 mg/ml), and the eyes were immediately enucleated and placed in oxygenated Ames' medium (Sigma, St. Louis, MO) at room temperature. Dissection and preparation of flat-mount retinas followed essentially the procedures described by others (Werblin, 1978; Wu, 1987). Oxygenated Ames' solution (adjusted at pH 7.3) was introduced continuously to the recording chamber, and the medium was maintained at 34°C by a temperature control unit (TC 324B; Warner Instruments, Hamden, CT). All pharmacological agents were dissolved in Ames' medium.

A photostimulator was used to deliver light spots (diameter of 600–1200 μm) to the retina via the epi-illuminator of the microscope. The intensity of unattenuated ($\log I = 0$) 500 nm light was 1.4×10^6 photons μm^{-2} sec^{-1}. The number of photoisomerizations per rod per second ($Rh^*rod^{-1}sec^{-1}$) was calculated by using a rod cross section of 0.5 μm^{-2} (Howes et al., 2002) and a rod integration time of 0.4 sec (Baylor, 1987). The peak amplitude of light-evoked current responses was plotted against light stimulus intensity, and data points were fitted by the Hill equation: $R/R_{max} = I^N/(I^N + \sigma^N) = 0.5[1 + \tanh 1.15N(\text{Log } I - \text{Log } \sigma)]$, where R is the current response amplitude, R_{max} is the maximum response amplitude, σ is the light intensity that elicits a half-maximal response, N is the Hill coefficient, tanh is the hyperbolic tangent function, and Log is the logarithmic function of base 10. In this article, we used the $R - \text{Log } I$ plot for our analysis (the right-hand term of the above equation), and, for such plots, the light intensity span [dynamic range (DR), range of intensity that elicits responses between 0.05 and 0.95% of R_{max}] of a cell equals to $2.56/N$ (Thibos and Werblin, 1978).

Voltage-clamp recordings. Voltage-clamp recordings were made with an Axopatch 200A amplifier connected to a DigiData 1200 interface and pClamp 6.1 software (Axon Instruments, Foster City, CA). Spike activities were recorded extracellularly with patch electrodes made with Narishige (Tokyo, Japan) or Sutter Instruments (Novato, CA) patch electrode pullers that were of 1–2 MΩ tip resistance when filled with Ames' medium in the loose-patch configuration. Whole-cell voltage-clamp recordings were made with patch electrodes of 5–7 MΩ tip resistance when filled with internal solution containing the following (in mM): 118 Cs methanesulfonate, 12 CsCl, 5 EGTA, 0.5 $CaCl_2$, 4 ATP, 0.3 GTP, 10 Tris, and 0.8 Lucifer yellow, adjusted to pH 7.2 with CsOH. The chloride equilibrium potential, E_{Cl}, with this internal solution was approximately −60 mV. Estimates of the liquid junction potential at the tip of the patch electrode before seal formation varied from −9.2 to −9.6 mV (Pang et al., 2002). For simplicity, we corrected all holding potentials by 10 mV. To determine the dark membrane potentials of ganglion cells, we measured the zero-current potentials of 12 α ganglion cells (including all three cell types described in this paper) with patch electrodes filled with Cs internal solution (above) and with potassium internal solution (Berntson and Taylor, 2000) and found that the zero-current potentials with K^+ were consistently 13–16 mV more hyperpolarized than with Cs^+. For cells recorded with only Cs^+, we corrected zero-current potential measured in darkness (dark membrane potential) by 15 mV. Because α ganglion cells have relatively large dendritic fields, it is possible that we were unable to control the voltage of the fine dendrites. We therefore selected cells with higher input resistance (>500 MΩ) when whole-cell recording was made and discarded any cell that showed unclamped spikes (typical from cells whose voltage at remote dendrites are not controlled).

Visualization of cell morphology. Three-dimensional cell morphology was visualized in flat-mount retinas through the use of Lucifer yellow fluorescence with a confocal microscope (model 510; Zeiss, Oberkochen, Germany). For vertical sections, retinas were subsequently fixed in fresh 4% paraformaldehyde with 0.05% gluderaldehyde for 15 min, transferred to 4% paraformaldehyde for another 2 hr, and then sectioned with a vibratome. Images were acquired with a 40× water immersion objective (numerical aperture, 1.20), using the 458 nm excitation line of an argon laser and a long-pass 505 nm emission filter. Consecutive optical sections were superimposed to form a single image using the Zeiss LSM-PC software, and these compressed image stacks were further processed in Adobe Photoshop 6.0 (Adobe Systems, San Jose, CA) to improve the signal-to-noise ratio. Because signal intensity values were typically enhanced during processing to improve visibility of smaller processes, the cell bodies and larger processes of some cells appear saturated attributable to their larger volume of fluorophore. Although background images of the retinal sections were acquired simultaneously with the fluorescent cells, they were imaged by using transmitted light. The level at which dendritic processes stratified in the inner plexiform layer (IPL) was characterized in retinal vertical sections by the distance from the processes to the distal margin (0%) of the IPL. α ganglion cells were identified by their three-dimensional morphology revealed by Lucifer yellow fluorescent images in retinal flat mounts and vertical sections: a large soma (20–25 μm in diameter) with an axon (therefore, we knew they were ganglion cells instead of displaced amacrine cells) and several stout primary dendrites emerging radially, and higher-order dendrites with a beaded appearance branching successively without significant crossing, with a dendritic field ~180–350 μm in diameter In vertical sections, dendrites of ON α ganglion cells (ONαGCs) stratified near 70% of the IPL depth, and those of the OFF α ganglion cells (OFFαGCs) stratified near 30% of the IPL depth (Peichl, 1989; Doi et al., 1995).

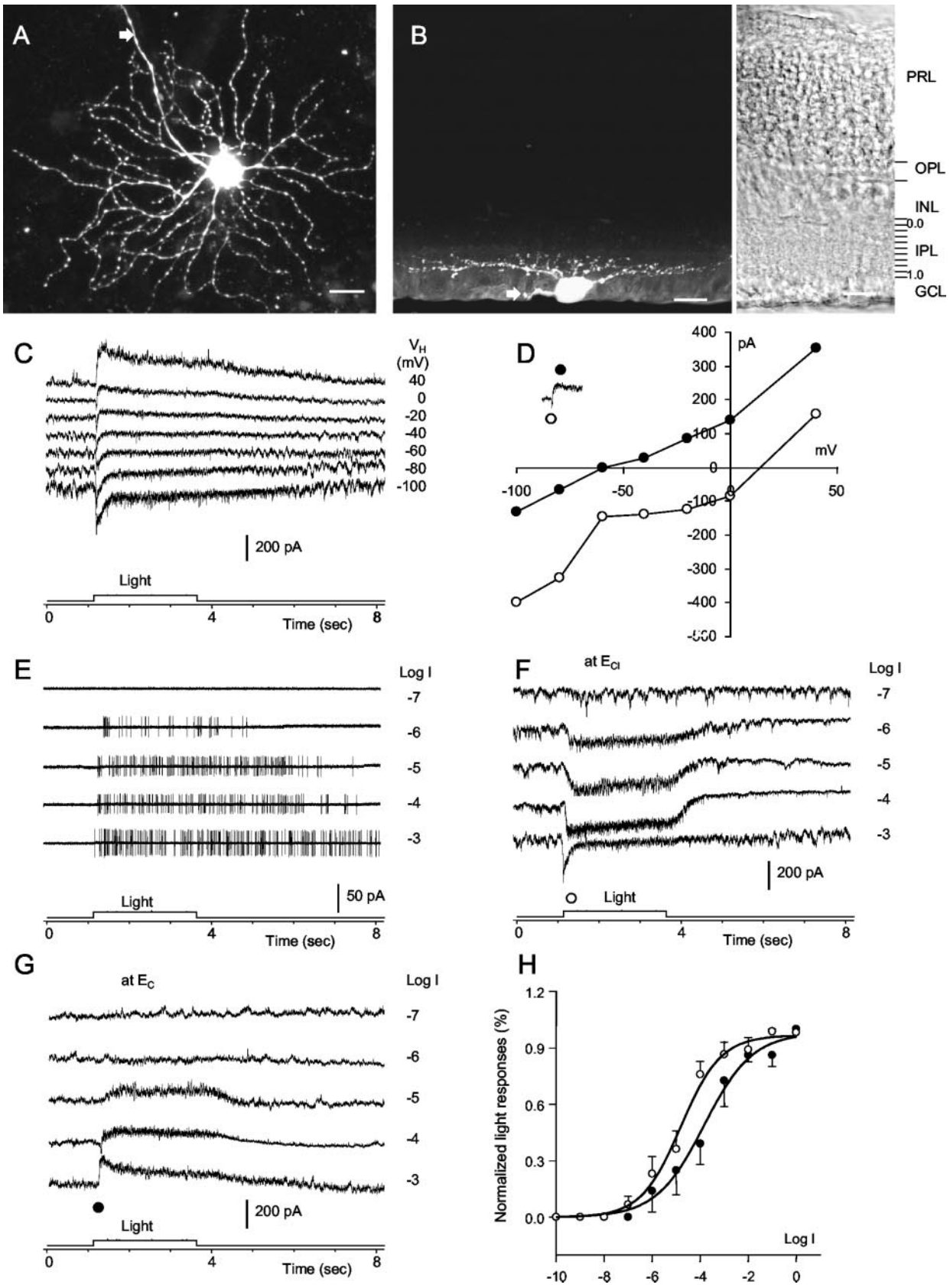

Figure 1. ONαGC. *A*, Stacked confocal fluorescent image in the flat-mount retina; *B*, image of the same cell in the vertical retinal section. Scale bars, 20 μm. PRL, Photoreceptor layer; OPL, outer plexiform layer; INL, inner nuclear layer; GCL, ganglion cell layer. *C*, Light-evoked current responses to a 2.5 sec light step (500 nm; $-3 = 700$ Rh*rod^{-1}sec^{-1}) at various holding potentials. *D*, Current–voltage relationships of the early (○) and late (●) component of the light responses. Spike activities (*E*), light-evoked excitatory cation current (ΔI_C) recorded at E_{Cl} (*F*), and light-evoked inhibitory chloride current (ΔI_{Cl}) recorded at E_C to 500 nm light steps (2.5 sec) of various intensities (*G*). *H*, Response–intensity relationships of the light-evoked cation and chloride currents [ΔI_C–Log *I* (○) and ΔI_{Cl}–Log *I* (●)]. The average dynamic range for ΔI_C is 4.9 log units and that for ΔI_{Cl} is 5.3 log units.

Results

Light responses of ONαGCs are mediated primarily by a cation current of mixed rod and cone inputs

Under infrared visual guidance in dark-adapted flat-mount mouse retinas, we selected ON ganglion cells, with large cell bodies that exhibited increased spike activity during light illumination with loose-patch electrodes. These cells were subsequently recorded with patch electrodes filled with internal solution and Lucifer yellow in the whole-cell voltage-clamp configuration. ONαGCs were identified by their three-dimensional morphology revealed by Lucifer yellow fluorescent images in retinal flat mounts and vertical sections (for details, see Materials and Methods). Figure 1, *A* and *B*, shows the stacked confocal fluorescent image of an ONαGC in the flatmount retina (*A*) and the image of the same cell in the vertical retinal section (*B*). The fluorescent images exhibited typical ONαGC morphology with dendrites stratifying near 70% of the IPL depth and a dendritic field of ~257 μm. The dendrites of all 28 ONαGCs we studied stratified near 65–80% of the IPL depth, with field diameters ranging from 210 to 335 μm. Figure 1*C* shows the light-evoked current responses of the same cell to a 2.5 sec light step recorded under dark-adapted conditions at various holding potentials. ONαGCs exhibited two light-evoked current components at the light onset. The early component (the peak inward current, marked with ○ in the inset in *D*) reversed near +10 mV [close to the equilibrium potential of a cation channel (E_C), as determined by the reversal potential of glutamate-induced current in the presence of 2 mM Co^{2+} (data not shown)] and the late component (the peak outward current, marked with ● in the inset in *D*) reversed near −60 mV [the equilibrium potential of the chloride channel (E_{Cl}); see Materials and Methods]. The current–voltage (*I–V*) relationships of these two current components (Fig. 1*D*) have positive slopes, indicating that they are associated with conductance increases. All 28 ONαGCs exhibited very similar response waveform, with the reversal potential of the early component ranging from −10 to 20 mV and that of the late component ranging from −46 to −61 mV. The average zero-current potential in darkness of these cells was −63 ± 6 mV (see Materials and Methods). Because ONαGCs in the mammalian retina received glutamatergic inputs from DBC_Cs and GABAergic–glycinergic inputs from amacrine cells (Pourcho and Owczarzak, 1989; Cohen et al., 1994; Qin and Pourcho, 1996; Brandstatter et al., 1998), the early component is likely to be mediated by bipolar cell inputs that gate a cation conductance, and the late component is likely mediated by amacrine cell inputs that gate a chloride conductance (Cohen and Miller, 1994).

To determine the relative rod–cone contribution to the ganglion cell light responses, we examined the light sensitivity of ONαGCs to 500 nm light steps under dark-adapted conditions. We used 500 nm light because mouse rods and cones exhibit the largest sensitivity difference near this wavelength (Lyubarsky et al., 1999), making it easier to distinguish between the two photoreceptor inputs to ganglion cells. Additionally, previous work and our preliminary data from the mouse retina have provided response thresholds and dynamic ranges of rods, rod bipolar cells, some cone bipolar cells, and amacrine cells to 500 nm lights, as well as the relative cone–rod sensitivity (Table 1, top). The threshold of dark-adapted mouse rods for 500 nm light is ~1.9 $Rh^*rod^{-1}sec^{-1}$ (Field and Rieke, 2002; Howes et al., 2002), and that of the M-cones is ~25–100 times higher (Baylor, 1987; Schneeweis and Schnapf, 1995; Lyubarsky et al., 1999). Because all mouse cones contain the M-pigment and most cones contain the S-pigment of various proportions (Applebury et al., 2000), these cells may be approximately divided into M-dominated (M/s) and S-dominated (S/m) cones, and the S-pigment is ~2 log units less sensitive to the 500 nm light than the M-pigment (Lyubarsky et al., 1999). The threshold of rod bipolar cells (DBC_R) in dark-adapted mouse retina is near 0.1–0.6 $Rh^*rod^{-1}sec^{-1}$ (Field and Rieke, 2002), with a dynamic range of ~2.2 log units (Berntson and Taylor, 2000). The dynamic range of the M/s cone ON bipolar cell (DBC_{MC}) response is much wider (~4 log units), and it consists of a rod input component with a response threshold near 1 $Rh^*rod^{-1}sec^{-1}$ (presumably mediated by rod–cone coupling and/or DBC_R–AII amacrine cell–DBC_C pathway) and a cone input component with a threshold ~2 log units higher (Berntson and Taylor, 2000). We recorded from two HBC_Cs that were more sensitive to 360 nm light than to 500 nm light (data not shown), and thus we believe that they are S/m cone bipolar cells (HBC_{SC}s). The threshold of these cells for 500 nm light was ~2000 $Rh^*rod^{-1}sec^{-1}$, and the dynamic range was 1.5 log units. We also recorded from seven AII amacrine cells (data are not shown but will be presented in a later publication), and the response threshold was ~0.001 $Rh^*rod^{-1}sec^{-1}$ and the dynamic range was 3.7 log units.

By comparing the response thresholds and dynamic ranges of preganglion cells with those of the α ganglion cells, we determined what types of bipolar cells and amacrine cells mediate α ganglion cell light responses. Figure 1*E–H* shows the spike activities (*E*), light-evoked excitatory cation current (ΔI_C) recorded at E_{Cl} (*F*), and light-evoked inhibitory chloride current (ΔI_{Cl}) recorded at E_C (*G*) of the same ONαGC (as in Fig. 1*A–D*) to 500 nm light steps (2.5 sec) of various intensities. In darkness, the cell exhibited no observable spontaneous spikes. The −7 light step elicited no spike response but a very small ΔI_C, whereas the −6 (0.7 $Rh^*rod^{-1}sec^{-1}$) light step gave rise to a burst of spikes and an inward ΔI_C of ~100 pA at E_{Cl}. As the light step became brighter, the spike train became longer and of higher frequency, and the inward ΔI_C became larger. We measured the light sensitivity of ΔI_C to 500 nm light in all 28 ONαGCs, and the average ± SD response–intensity (ΔI_C–Log *I*) relationsships are plotted in Figure 1*H* (○). The solid curve was fitted by the Hill equation

Table 1. Response thresholds and dynamic ranges of various mouse retinal neurons

	Threshold (500 nm, $Rh^*rod^{-1}sec^{-1}$)	Dynamic range (log unit)	Dark V_m (mV)
Rod	1.9 (f.r.)	2.0 (f.r.)	
Cone (M/s)	48–190 (b.)	2.0	
Cone (S/m)	1000–2000 (1.et al)	2.0	
DBC_R	0.1–0.6 (f.r.)	1.7–2.2 (b.t. and f.r.)	
DBC_{MC}/HBC_{MC}	0.1–10 (b.t., f.r. and p.w.)	4.0 (b.t.)	
HBC_{SC}	2213 (p.w.)	1.5 (p.w.)	
AII	0.001 (p.w.)	3.7 (p.w.)	

	ONΔI_C	OFFΔI_C	ΔI_{Cl}	Spike	ONΔI_C	OFFΔI_C	ΔI_{Cl}	
ONαGC	0.044		0.1	0.047	4.9		5.3	−63 ± 6
tOFFαGC	1.1	1397	2.2	1813	3.9	1.6	3.3	−61 ± 7
sOFFαGC	0.55		0.0022	0.007	3.0		5.9	−51 ± 5

Top, Values of response thresholds and dynamic ranges of mouse rods, M-pigment-dominated cones [cone (M/s)], S-pigment-dominated cones [cone (S/m)], rod depolarizing bipolar cells (DBC_R), M-cone-dominated depolarizing bipolar cells (DBC_{MC}), S-cone-dominated hyperpolarizing bipolar cells (HBC_{SC}), and all amacrine cells (AIIAC) derived from previous publications or our unpublished data. Light intensity required to elicit a threshold step response was calculated from flash response threshold by a rod integration time of 0.4 seconds. (f.r.), Field and Rieke, 2002; (b.), Baylor, 1987; (b.t.), Berntson and Taylor, 2000; (l.et al), Lyubarsky et al., 1999; (p.w.), Pang and Wu, unpublished data. Bottom, Summary of average response thresholds and dynamic ranges of ΔI_C, ΔI_{Cl}, and spike responses of ONαGCs, tOFFαGCs, and sOFFαGCs obtained in this study. The average ± SD dark membrane potentials of the three types of αGCs are also listed in the right column.

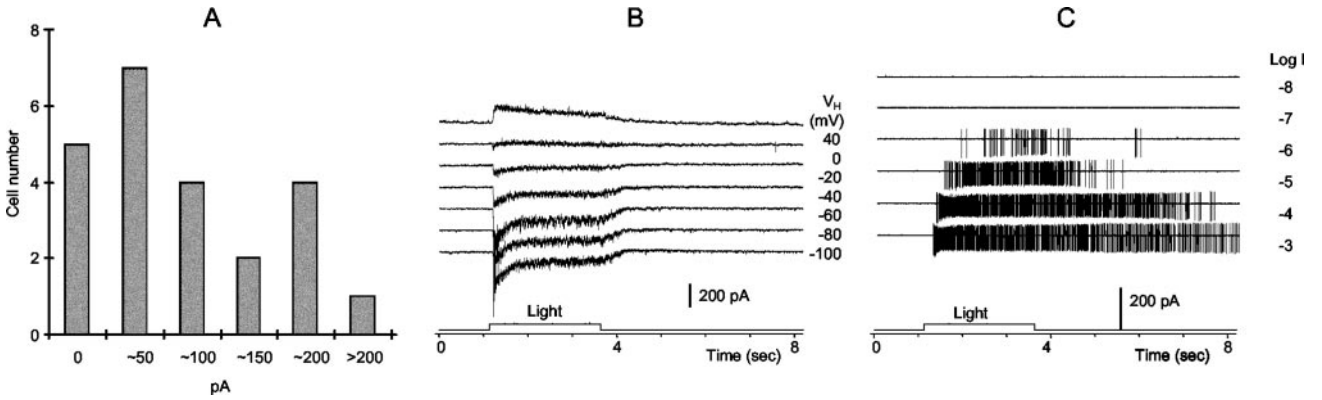

Figure 2. ΔI_{Cl} amplitude and ONαGC responses. *A*, Histogram of ΔI_{Cl} amplitude of 23 ONαGCs; *B*, light-evoked current responses of an ONαGC (whose ΔI_{Cl} peak amplitude was 3 pA) to a 2.5 sec light step (500 nm; $-3 = 700$ Rh*rod^{-1}sec^{-1}) at various holding potentials; *C*, the spike responses to 500 nm, 2.5 sec light steps of various intensities of the same cell.

(see Materials and Methods). The average threshold (defined as eliciting 5% of the maximum response) was near -7.2 (0.044 Rh*rod^{-1}sec^{-1}), and the dynamic range was 4.9 log units. Our data demonstrate that the dynamic range and response threshold of ΔI_C in mouse ONαGCs are close to those of the DBC_{MC} (Table 1), which have mixed rod/M-cone signals [two limbs in the response intensity curve (Berntson and Taylor, 2000)], consistent with the idea that the primary light-evoked excitatory inputs in ONαGCs are mediated by the cone ON bipolar cells (Bloomfield and Miller, 1986; Bloomfield and Dacheux, 2001).

The average threshold of light-evoked inhibitory current ΔI_{Cl} of the 28 ONαGCs was -6.8 (0.1 Rh*rod^{-1}sec^{-1}), and the average $\pm$ SD response–intensity (ΔI_{Cl}–Log I) relationship (shown in Fig. 1*H*, ●) had an average dynamic range of 5.3 log units. This indicates that the amacrine cells mediating ΔI_{Cl} of ONαGCs have similar rod–cone signals (we named these cells AC_{M1}) as the DBC_{MC}s, with a slightly lower threshold and wider dynamic range. In all ONαGCs, the threshold of light-evoked spike activities (0.047 $\pm$ 0.005 Rh*rod^{-1}sec^{-1}) was closer to that of the ΔI_C than to ΔI_{Cl}. This is consistent with our observation that the dark resting potential of the ONαGCs (-63 ± 6 mV) are very close to E_{Cl}, and thus the spiking signals of the cells are predominately mediated by ΔI_C from DBC_{MC} inputs. Average response thresholds and dynamic range as well as the dark membrane potentials of ONαGCs are listed in Table 1 (bottom).

Light-evoked chloride currents from amacrine cells shunt ONαGC light responses

Despite the homogeneity in the threshold and dynamic range of light-evoked spikes, ΔI_C and ΔI_{Cl} in all ONαGCs, the strength (amplitude) of ΔI_{Cl} varied from cell to cell. Figure 2*A* shows histograms of the peak ΔI_{Cl} amplitudes of 23 dark-adapted ONαGCs. The amplitude of ΔI_{Cl} in approximately one-half of the ONαGCs was <50 pA, whereas that of the other one-half was between 60 and 300 pA. There were no noticeable differences in the cell morphology, response sensitivity, ΔI_C amplitude, or *I–V* relationships between those cells with large ΔI_{Cl} and those with small ΔI_{Cl}. However, the frequency of light-evoked spikes in ONαGCs with small ΔI_{Cl} was consistently higher than that with larger ΔI_{Cl}. Figure 2*B* shows light-evoked current responses at different potentials in an ONαGC with small ΔI_{Cl}, and Figure 2*C* shows the spike responses to 500 nm light of different intensities. The ΔI_{Cl} measured at $E_C = +12$ mV was ~3 pA, and the spike activities of the cell exhibited the same threshold (-6.3) to 500 nm light as the cell in Figure 1 that had a larger ΔI_{Cl}; however, the cell displayed a higher spike frequency. Light-elicited spike frequency of the five ONαGCs with $\Delta I_{Cl} < 10$ pA was approximately two to five times higher than those ONαGCs with larger ΔI_{Cl}. This inverse relationship between spike frequency and ΔI_{Cl} suggests that an important function of amacrine cell (AC_{M1}) inputs (associated with a chloride conductance increase) to ONαGCs is to shunt the voltage responses elicited by ΔI_C from bipolar cell inputs. Variations of AC_{M1} inputs result in a spectrum of light spike response frequencies in various ONαGCs.

Light responses of transient OFFαGCs are mediated primarily by a transient cation current from S-cone-driven bipolar cells

By using the same experimental procedures, we studied light responses of 32 OFF α ganglion cells. Two major types of OFF response patterns were observed, although the morphology of these cells was very similar. The first type was quiet in darkness (no spontaneous spikes), and they exhibited transient spike activities only at the cessation of the light step [we named these cells transient OFF cells (tOFFαGCs)], whereas the second type exhibited spontaneous spikes in darkness and a sustained reduction of spike activity during the light illumination [we named these cells sustained OFF cells (sOFFαGCs)]. Among the 32 OFF α-like ganglion cells from which we recorded, 12 showed tOFFαGC responses and 20 displayed sOFFαGC responses.

Figure 3*A–D* shows the stacked confocal fluorescent image of a tOFFαGC in the flat-mount retina (*A*), the image of the same cell in vertical retinal section (*B*), the light-evoked current responses to a 2.5 sec 500 nm light step recorded under dark-adapted conditions at various holding potentials (*C*), and the current–voltage relationships of the responses at light onset and offset (*D*). The fluorescent images in *A* and *B* exhibited typical OFF α-cell-like morphology with dendritic field diameter ranging from 180 to 250 μm, and dendrites stratified near 30% (instead of 70% in the ONαGCs) of the IPL depth (Peichl, 1989; Doi et al., 1995). The baseline currents at -60 mV or below were very smooth, except for a few small transient inward current bumps [spontaneous EPSCs (sEPSCs)] mediated by spontaneous release of glutamatergic vesicles (Tian et al., 1998). The baseline currents at -40 mV or above, however, were much noisier, with many transient outward currents [spontaneous IPSCs (sIPSCs)]. This abrupt voltage-dependent increase of sIPSCs occurred between -40 and -60 mV and was consistent in all OFF α ganglion cells (both tOFFαGCs and sOFFαGCs; see below). At negative holding potentials (-60 to -100 mV), the light step elicited small

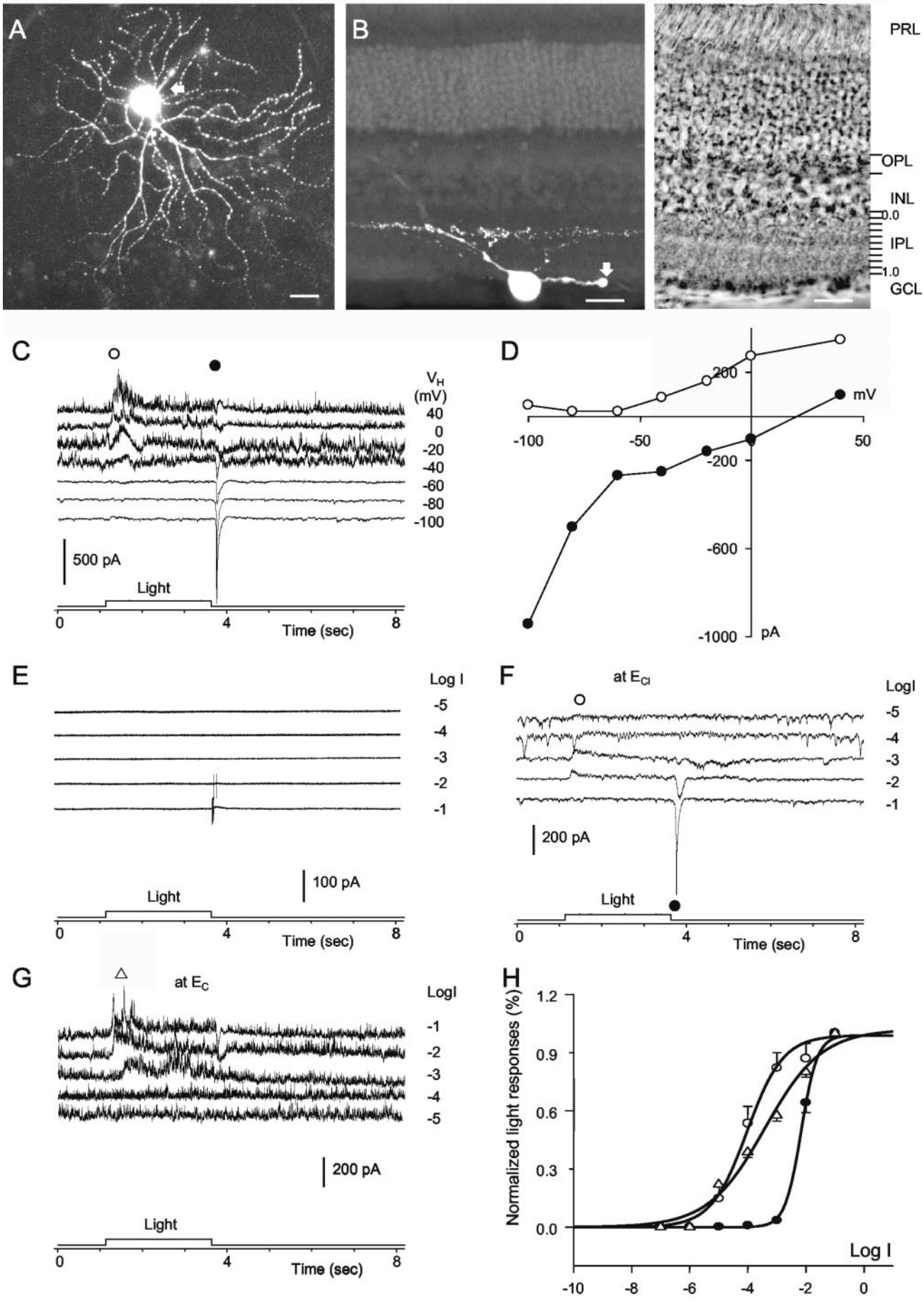
A
B
PRL
OPL
INL
0.0
IPL
1.0
GCL
C
V_H (mV)
40
0
-20
-40
-60
-80
-100
500 pA
Light
0
4
8
Time (sec)
D
200
mV
-100
-50
50
-200
-600
-1000
pA
E
Log I
-5
-4
-3
-2
-1
100 pA
Light
0
4
8
Time (sec)
F
at E_{Cl}
LogI
-5
-4
-3
-2
-1
200 pA
Light
0
4
8
Time (sec)
G
at E_C
LogI
-1
-2
-3
-4
-5
200 pA
Light
0
4
8
Time (sec)
H
Normalized light responses (%)
1.2
0.9
0.6
0.3
0.0
Log I
-10
-8
-6
-4
-2
0

outward current responses at the onset and a large transient inward current at the offset. The ON response became larger at more positive potentials, and it did not exhibit a reversal potential between −100 and +60 mV, suggesting that it may be mediated by two opponent conductance changes: a cation conductance decrease at the HBC–tOFFαGC synapse and a chloride conductance increase at the AC–tOFFαGC synapse. The OFF response was a transient inward current at negative potentials, it became smaller as the holding potential became more positive, and it reversed near +20 mV (E_C). All 12 tOFFαGCs exhibited very similar baseline noise and ON and OFF light responses with the E_C values for the OFF response varying from −10 to +25 mV. The average zero-current potential in darkness of these cells was −61 ± 7 mV. These results suggest that the OFF response of the tOFFαGC is probably mediated by a cation conductance (with reversal potential near 0 mV), a mechanism that is consistent with anatomical results, suggesting that OFF α ganglion cells in mammalian retinas receive synaptic inputs from the OFF cone bipolar cells (HBC_Cs) (Bloomfield and Dacheux, 2001).

Figure 3*E–G* shows the spike activities (*E*), ΔI_C (*F*), and ΔI_{Cl} recorded at E_C (*G*) of a tOFFαGC to 500 nm light steps (2.5 sec) of various intensities. In darkness, the cell exhibited no observable spontaneous spikes but some sEPSCs. The −5 step elicited no spiking activities and a very small ON ΔI_C, whereas the −4 and −3 light steps evoked no spikes and larger outward ON ΔI_C. Brighter light steps (−2 and −1) elicited a brief train of spikes and a transient OFF inward ΔI_C, in addition to the outward ON ΔI_C. We measured the light sensitivity of OFF ΔI_C to 500 nm light in all tOFFαGCs, and the average ± SD response–intensity (OFF ΔI_C–Log *I*) relationships are plotted in Figure 3*H* (●). The solid curve was fitted by the Hill equation. The average threshold was near −2.7 (1394 Rh*rod^{-1}sec^{-1}), and the dynamic range was 1.6 log units. The average spike response threshold was 1813 ± 470 Rh*rod^{-1}sec^{-1}, indicating that the spike response of these cells are mediated by the OFF ΔI_C. Because the OFF ΔI_C and spike response threshold and dynamic range are very close to those of the HBC_{SC}s (Table 1), we believe that they are primarily mediated by the S/m cones through the S/m cone hyperpolarizing bipolar cells.

"Silent" bipolar cell inputs to tOFFαGCs at light onset

The threshold of the ON ΔI_C (Fig. 3*F*,*H*, ○) was approximately −5, which was ~2–3 log units higher than that of the OFF ΔI_C and spike responses. We measured the light sensitivity of ON ΔI_C to 500 nm light in all 12 tOFFαGCs, and the average ± SD response–intensity (ON ΔI_C–Log *I*) relationship is plotted (and fitted by the Hill equation) in Figure 3*H* (○). The average threshold was near −5.8 (1.1 Rh*rod^{-1}sec^{-1}), and the average dynamic range was 3.9 log units. By comparing these results with the parameters listed in Table 1, we believe that the ON ΔI_C of tOFFαGCs is mediated primarily by HBC_{MC}s. It is important to note that ON ΔI_C is an outward current that results in membrane hyperpolarization and decrease of spike activity. Therefore, because tOFFαGCs do not exhibit spontaneous spike activities in darkness (Fig. 3*E*), ON ΔI_C cannot decrease spiking further, and thus it has no physiological consequences on the tOFFαGC output and can be considered as a silent bipolar cell input.

Silent amacrine cell inputs to tOFFαGCs

The average threshold of ΔI_{Cl} elicited by 500 nm light from 12 tOFFαGCs was −5.5 (2.2 Rh*rod^{-1}sec^{-1}), and the average ± SD response–intensity (ΔI_{Cl}–Log *I*) relationships (Fig. 3*H*) had a dynamic range of 3.3. Comparing these results with the parameters listed in Table 1 reveals that the ΔI_{Cl} of tOFFαGCs is probably mediated by amacrine cells with mixed rod and cone inputs (we named these cells AC_{M2}, which receive inputs from M-cone bipolar cells with mixed rod) [possibly through rod–cone coupling and/or AII amacrine cells (Demb and Pugh, 2002)] and M-cone inputs. Because the average zero-current potential in darkness of these cells was −61 ± 7 mV, a value very close to E_{Cl}, the AC_{M2}-mediated current response (ΔI_{Cl}) contributes little to the total light-evoked current. Moreover, because tOFFαGCs do not exhibit spontaneous spike activities in darkness (Fig. 3*E*) and ΔI_{Cl} returns to the baseline before the onset of the transient inward OFF ΔI_C (Fig. 3*F*,*G*; for shorter light stimuli, OFF ΔI_C was much smaller), the shunting action of ΔI_{Cl}-mediated conductance increase causes little physiological consequence to the tOFFαGC output and can be considered as a silent amacrine cell input.

Average response thresholds and dynamic range as well as the dark membrane potentials of ON ΔI_C, OFF ΔI_C, and ΔI_{Cl} of the tOFFαGCs are listed in Table 1 (bottom).

Light responses of sOFFαGCs are mediated by both a cone-driven bipolar cell input and a rod-driven amacrine cell input

Figure 4*A–C* shows the stacked confocal fluorescent image of a sustained sOFFαGC in the flat-mount retina (*A*), the image of the same cell in vertical retinal section (*B*), and the light-evoked current responses to a 500 nm 2.5 sec light step recorded under dark-adapted conditions at various holding potentials (*C*). The fluorescent images in *A* and *B* exhibited typical OFF α ganglion cell morphology with dendrites stratified near 30% of the IPL depth (Peichl, 1989; Doi et al., 1995). Similar to the tOFFαGCs, the baseline currents at −60 mV or below were relatively smooth and at −40 mV or above were much noisier, possibly attributable to electrical coupling with amacrine cells that release GABAergic or glycinergic vesicles onto the recorded cell (Xin and Bloomfield, 1997) (see Discussion). The light step gave rise to a transient outward current followed by a sustained outward current at all potentials (without a reversal potential), and the current–voltage relationships of the peak and steady-state light responses are shown in Figure 4*D*. The lack of reversal potential suggests that the light response is probably mediated by two opponent conductance changes, a cation conductance decrease at the HBC–sOFFαGC synapse and a chloride conductance increase at the AC–sOFFαGC synapse. The sustained outward current lasted for seconds after light offset and then exhibited one to two transient dips (Fig. 4*C*). All 20 sOFFαGCs exhibited very similar baseline noise and light response patterns, and the average zero-current potential in darkness of these cells was −51 ± 7 mV. A major

←

Figure 3. tOFFαGC. *A*, Stacked confocal fluorescent image in the flat-mount retina; *B*, image of the same cell in the vertical retinal section. Scale bars, 20 μm. PRL, Photoreceptor layer; OPL, outer plexiform layer; INL, inner nuclear layer; GCL, ganglion cell layer. *C*, Light-evoked current responses to a 2.5 sec light step (500 nm; −2 = 7000 Rh*rod^{-1}sec^{-1}) at various holding potentials; *D*, current–voltage relationships of the ON (○) and OFF (●) responses. Spike activities (*E*), light-evoked excitatory cation current (ΔI_C) recorded at E_{Cl} (*F*), and light-evoked inhibitory chloride current (ΔI_{Cl}) recorded at E_C to 500 nm light steps (2.5 sec) of various intensities (*G*). *H*, Response–intensity relationships of the light-evoked cation and chloride currents [ON ΔI_C–Log *I* (○), OFF ΔI_C–Log *I* (●), and ON ΔI_{Cl}–Log *I* (▲)]. The average dynamic range for ON ΔI_C is 3.9 log units, that for the OFF ΔI_C is 1.6 log units, and that for ΔI_{Cl} is 3.3 log units.

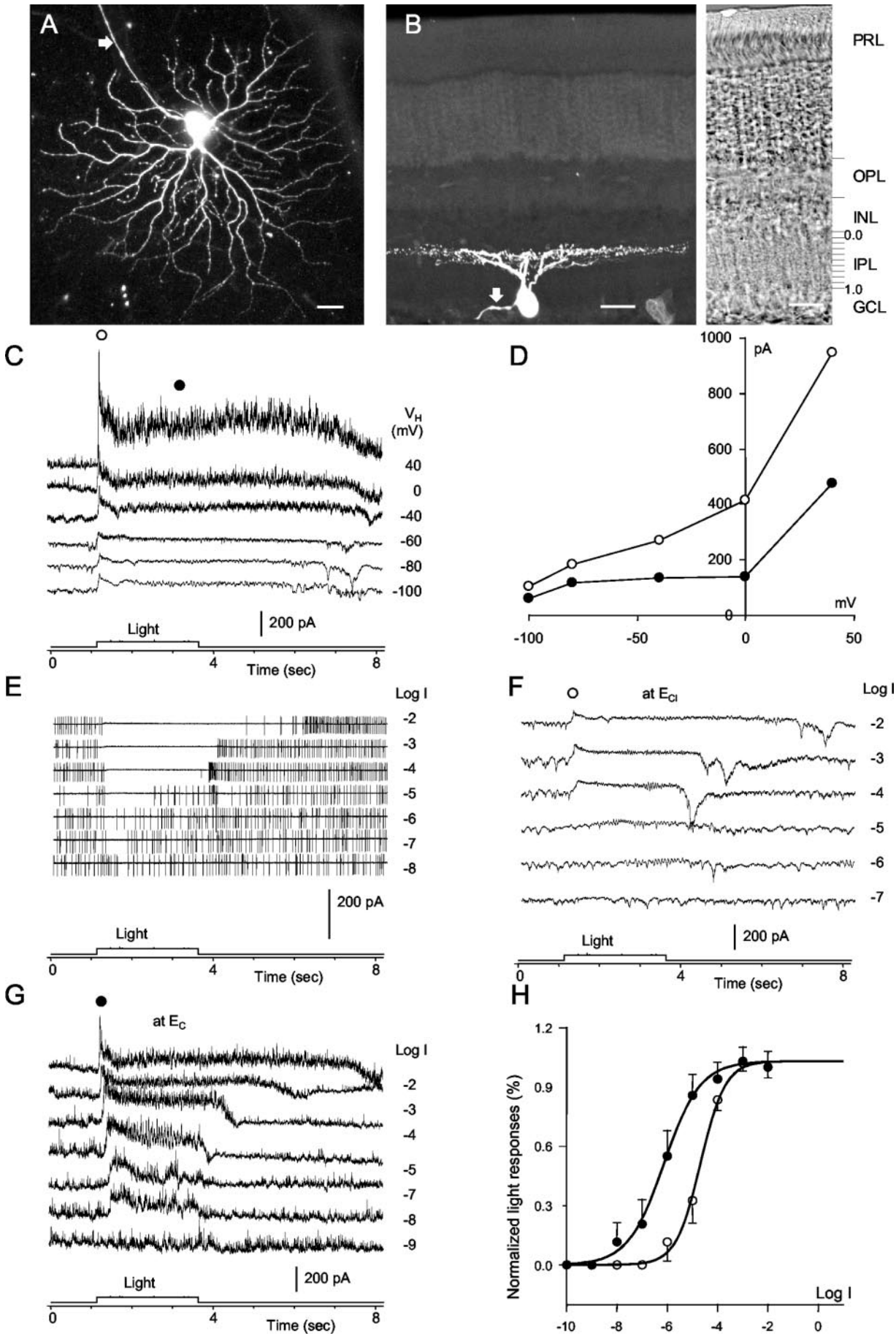
A
B
PRL
OPL
INL
0.0
IPL
1.0
GCL
C
V_H (mV)
40
0
-40
-60
-80
-100
Light
200 pA
0
4
8
Time (sec)
D
pA
1000
800
600
400
200
0
mV
-100
-50
0
50
E
Log I
-2
-3
-4
-5
-6
-7
-8
200 pA
Light
0
4
8
Time (sec)
F
at E_{Cl}
Log I
-2
-3
-4
-5
-6
-7
Light
200 pA
0
4
8
Time (sec)
G
at E_C
Log I
-2
-3
-4
-5
-7
-8
-9
Light
200 pA
0
4
8
Time (sec)
H
Normalized light responses (%)
1.2
0.9
0.6
0.3
0.0
Log I
-10
-8
-6
-4
-2
0

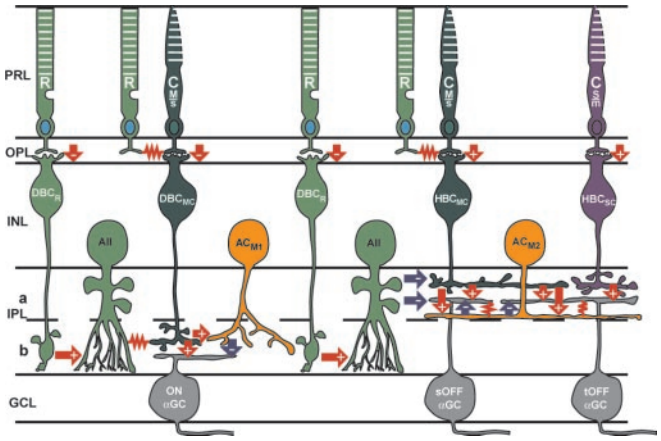

Figure 5. Synaptic circuit diagram of the ONαGCs, tOFFαGCs, and sOFFαGCs in the mouse retina. R, Rods; C(M/s), M-pigment-dominated cones; C(S/m), S-pigment-dominated cones; DBC_R, rod depolarizing bipolar cell; DBC_{MC}, M-cone-dominated depolarizing bipolar cell; HBC_{MC}, M-cone-dominated hyperpolarizing bipolar cell; HBC_{SC}, S-cone-dominated bipolar cells; AII, AII amacrine cells; AC_{M1}, amacrine cell with mixed rod– cone inputs in the ONαGC pathway; AC_{M2}, amacrine cell with mixed rod– cone inputs in the OFFαGC pathway; arrows, chemical synapses (red, glutamatergic; blue, GABAergic/glycinergic; + sign, preserving; and − sign, inverting); ⁓ (red), electrical synapses; PRL, photoreceptor layer; OPL, outer plexiform layer; INL, inner nuclear layer; IPL, inner plexiform layer (a, sublamina a; b, sublamina b); GCL, ganglion cell layer.

difference between the tOFFαGCs and sOFFαGC is that sOFFαGCs did not show the transient inward current at light offset (compare Figs. 3*C*, 4*C*).

Figure 4 *E–H* shows the spike activities (*E*), ΔI_C (*F*), and ΔI_{Cl} (*G*) of the same sOFFαGC as in Figure 4 *A–D* to 500 nm light steps (2.5 sec) of various intensities. In darkness, the cell exhibited spontaneous spikes of ~5–10 Hz and some sEPSCs at E_{Cl}. The −8 step resulted in a very brief period of decrease in spiking activities, elicited no ΔI_C, but evoked a sustained outward ΔI_{Cl}. The −7 light step decreased the spike frequency for ~0.7 sec, elicited no ΔI_C, and evoked a larger ΔI_{Cl}. Brighter light steps resulted in longer periods of spike decrease and larger ΔI_{Cl}, and, at −5, light started to elicit ΔI_C. As the light step became even brighter, the decrease of spike activity lasted longer, and ΔI_C and ΔI_{Cl} became larger and longer. We measured the light sensitivity of ΔI_C and ΔI_{Cl} to 500 nm light in all 20 sOFFαGCs, and the average ± SD response–intensity (ΔI_C–Log *I* and ΔI_{Cl}–Log *I*) relationships are plotted and fitted with the Hill equation in Figure 4 *H*. The average threshold for ΔI_C was near −6.1 (0.55 Rh*rod^{-1}sec^{-1}) with a dynamic range of 3.0 log units, and the average threshold for ΔI_{Cl} was near −8.5 (0.0022 Rh*rod^{-1}sec^{-1}) with a dynamic range of 5.9 log units. The average threshold of the spike decrease was −8.0 (0.007 Rh*rod^{-1}sec^{-1}). These results suggest that ΔI_C of sOFFαGCs is probably mediated by HBC_{MC}s, similar to the bipolar cells that mediate ΔI_C in tOFFαGCs. ΔI_{Cl} of sOFFαGCs is likely to be mediated by the AII amacrine cells who have very high sensitivity to 500 nm lights (Table 1). Because the dynamic range of ΔI_{Cl} is much wider than that of the AII ACs, another AC with mixed rod and cone inputs (possibly AC_{M2}) may also be involved in mediating ΔI_{Cl} in sOFFαGCs. Because the threshold of spike response was closer to ΔI_{Cl} than to ΔI_C, ΔI_{Cl} should contribute significantly more to the spike responses. This may be partially explained by our observation that the average dark membrane potential of sOFFαGCs was near −51 mV, ~10 mV more depolarized than E_{Cl}. This is in contrast to the ONαGCs and tOFFαGCs whose average dark membrane potentials are much closer to E_{Cl}, and thus, in these cells, ΔI_{Cl} could only contribute to the light response by voltage shunting. The difference in dark membrane potential may also explain why sOFFαGCs exhibit spontaneous spikes in darkness whereas ONαGCs and tOFFαGCs do not.

Average response thresholds and dynamic range as well as the dark membrane potentials of ON ΔI_C and ΔI_{Cl} of the sOFFαGCs are listed in Table 1 (bottom).

Discussion

Mouse α ganglion cells exhibit three distinct types of light responses: ON, transient OFF, and sustained OFF

By using loose-patch, whole-cell voltage-clamp and Lucifer yellow fluorescent techniques, we studied the light responses of 51 ganglion cells with α-cell-like morphology in dark-adapted mouse retina and found that they can be clearly divided into three types. The first type, the ONαGCs, exhibits no spike activity in darkness, increased spikes in light, sustained light-evoked inward cation current (ΔI_C) at E_{Cl}, sustained light-evoked chloride current (ΔI_{Cl}) of varying amplitude at E_C, and large soma (20–25 μm in diameter) with α-cell-like dendritic field ~180–350 μm stratifying near 70% of the IPL depth. The second type, the tOFFαGCs, exhibit no spike activity in darkness, transient increased spikes at light offset, small sustained light-evoked outward ΔI_C in light and large transient inward ΔI_C at light offset, and a sustained outward ΔI_{Cl} in light. Morphologically, the tOFFαGCs are similar to the ONαGCs except for that their dendrites stratified near 30% of the IPL depth. The third type, the sOFFαGCs, exhibit maintained spike activity of 5–10 Hz in darkness, sustained decrease spikes in light, sustained outward ΔI_C, sustained outward ΔI_{Cl} in light, and a morphology similar to the tOFFαGCs.

Our data agree with the ON and OFF sublaminar rule of the retinal IPL very well: ganglion cells with dendrites ramified in sublamina A display OFF responses and those with dendrites in sublaminar B display ON responses (Nelson et al., 1978). On the other hand, α ganglion cells in mammalian retinas are believed to have transient light responses (Cleland et al., 1975; Peichl and Wassle, 1981; Saito, 1983); however, in the mouse retina, we found that only one-quarter of the α ganglion cells are transient (tOFFαGCs). This difference may result from species difference or different adaptational conditions (all of our recordings were performed under infrared illumination). Alternatively, because the transient light responses described in previous studies are correlated with ganglion cells of large somas without detailed dendritic morphology, they may represent other populations of ganglion cells with large somas.

←

Figure 4. sOFFαGC. *A*, Stacked confocal fluorescent image in the flat-mount retina; *B*, image of the same cell in the vertical retinal section. Scale bars, 20 μm. PRL, Photoreceptor layer; OPL, outer plexiform layer; INL, inner nuclear layer; GCL, ganglion cell layer. *C*, Light-evoked current responses to a 2.5 sec light step (500 nm; −2 = 7000 Rh*rod^{-1}sec^{-1}) at various holding potentials; *D*, current–voltage relationships of the peak (○) and steady-state component (●) of the light responses. Spike activities (*E*), light-evoked excitatory cation current (ΔI_C) recorded at E_{Cl} (*F*), and light-evoked inhibitory chloride current (ΔI_{Cl}) recorded at E_C to 500 nm light steps (2.5 sec) of various intensities (*G*). *H*, Response–intensity relationships of the light-evoked peak cation and chloride currents [ΔI_C–Log *I* (○) and ΔI_{Cl}–Log *I* (●). The average dynamic range for ΔI_C is 3.0 log units, and that for ΔI_{Cl} is 5.9 log units.

Synaptic circuitries of αGCs: each type of αGCs receive light-evoked signals from BCs and ACs with different rod/cone inputs

In this study, we used the whole-cell voltage clamp technique to separate the light-evoked BC and AC inputs (ΔI_C and ΔI_{Cl}, respectively) to αGCs. By comparing the response threshold and dynamic ranges of ΔI_C and ΔI_{Cl} and spike activities of each type of αGCs with the corresponding parameters of preganglion cells, we proposed a functional synaptic circuitry of the BC and AC inputs to αGCs (Fig. 5). It is worth noting that this circuitry diagram includes a minimum number of circuit components, although our data may also be explained by more complex schemes. The outlines of our proposed circuitry are consistent with the general plan set forth by anatomical analysis but with several new and more detailed findings revealing how synapses in the inner retina function.

We found that the light responses of ONαGCs are quite homogenous, and they all appear to receive excitatory inputs from DBC_{MC}s, which give a mixed rod/M-cone signal with a rod-like threshold and a wide (combined rod–cone) dynamic range. The rod signals are mediated by either the rod–DBC_R–AII–DBC_C (ON1) pathway or the rod–cone–DBC_C (ON2) pathway (Bloomfield and Dacheux, 2001; Demb and Pugh, 2002), and the cone signals are mediated directly by the M-cone–DBC_{MC} synapse. In all 28 ONαGCs, we never observed a response threshold higher then 20 $Rh^*rod^{-1}sec^{-1}$ or an operating range beyond 1000 $Rh^*rod^{-1}sec^{-1}$, suggesting that the contribution of the S-cone inputs is minor. The only significant variation among ONαGCs is their spike response frequency and the amplitude (not the threshold or dynamic range) of ΔI_{Cl}. Because the dark membrane potential of these ganglion cells is close to E_{Cl}, we suggest that the primary function of the amacrine cell (AC_{M1}) input is to shunt the DBC_{MC}-mediated input. The inverse relationship between ΔI_{Cl} amplitude and the frequency of light-evoked spikes in the ONαGCs supports this notion.

Our finding that all ONαGCs exhibit homogenous response–intensity function (Fig. 1*H*) contrasts a recent study that reports four groups of ON ganglion cells in the mouse retina, each having a distinct response–intensity curve (Deans et al., 2002). Because responses of these ganglion cells were recorded with extracellular electrodes and the cell morphology was not revealed, the four groups may reflect both α and non-α ON ganglion cells (and perhaps spiking displaced amacrine cells). On the basis of the response threshold and dynamic range, it appears that ONαGCs belong to the groups with intermediate sensitivity and wide operating range (mixed rod–cone inputs) and not those of high (rod driven) or low sensitivity (cone driven).

The two types of OFFαGCs display drastically different responses, and thus their BC and AC inputs are different. tOFFαGCs exhibit transient increase of spikes at light offset with a very high threshold, and the sOFFαGCs exhibit spike decrease when the light is turned on with an extremely low threshold. These cells seem to receive two excitatory bipolar cell inputs: one is mediated by a sustained HBC with an M-cone-dominated signal and the other by a transient HBC (with an off overshoot response) with an S-cone-dominated signal (J.-J. Pang and S. M. Wu, unpublished data) and an AC input with mixed rod/M-cone inputs (AC_{M2}). The HBC_{SC}-mediated transient OFF ΔI_C is responsible for the transient OFF spike response. The HBC_{MC}-mediated ON ΔI_C and AC-mediated ΔI_{Cl} are both inhibitory (because they are outward currents), and, because tOFFαGCs do not exhibit spontaneous spikes in darkness, these outward currents do not serve much physiological function (silent synapses). On the other hand, sOFFαGC responses are extremely sensitive to 500 nm light, with a threshold lower than HBC_{MC}s and even lower than HBC_Rs (Field and Rieke, 2002). It appears that sOFFαGC responses are mediated primarily by the AII AC-mediated ΔI_{Cl}, which has a threshold of near 0.001 $Rh^*rod^{-1}sec^{-1}$ (Pang and Wu, unpublished data) at the low light intensity range. An HBC_{MC}-mediated ΔI_C is also involved in mediating the spike responses of the cells at higher light intensities. These results also suggest that the feedforward synapse from AII AC to sOFFαGCs are stronger (or of higher gain) than the feedback synapse from AII AC to HBC_{MC}s and the electrical synapse between AII AC and DBC_{MC}s (Fig. 5), because the AII response to dim light (below 0.01 $Rh^*rod^{-1}sec^{-1}$) could only be observed in ΔI_{Cl} of the sOFFαGCs.

A major difference between sOFFαGCs and the other two types of αGCs is that sOFFαGCs exhibit spontaneous spike activity of 5–10 Hz in darkness, whereas the other αGCs do not. This can be partially explained by our finding that sOFFαGCs have an average dark membrane potential (-51 ± 7 mV) ~10 mV more positive than the other two types of αGCs (-63 ± 6 and -61 ± 7 mV for the ONαGCs and tOFFαGCs, respectively). Another factor that may contribute to the spontaneous spiking in sOFFαGCs is that it has been shown, at least in the salamander retina, that the sustained OFF bipolar cells exhibit large sEPSCs in darkness (Wu et al., 2000). These sEPSCs in HBCs may trigger sEPSCs in sOFFαGCs. As sOFFαGCs are maintained at a relatively more depolarized voltage in darkness, large sEPSCs may depolarize the cell above the threshold of action potentials and thus cause spontaneous spike activities.

In our voltage-clamp experiments, we found an abrupt voltage-dependent increase of sIPSCs that occurred between −60 and −40 mV in all OFFαGCs (both tOFFαGCs and sOFFαGCs) but not in ONαGCs. One possible explanation for this abrupt voltage-dependent increase of sIPSCs is that the depolarizing current needed to maintain the positive holding potential may leak into amacrine cells through gap junctions (Xin and Bloomfield, 1997), which would facilitate the release of GABAergic or glycinergic vesicles from amacrine cells to the recorded ganglion cell (Tian et al., 1998). Anatomical studies have shown that reciprocal electrical synapses exist between OFFαGCs and GABAergic ACs in mammalian retinas (Dacey and Brace, 1992; Jacoby et al., 1996; Bloomfield and Xin, 1997). Our voltage-clamp results suggest that membrane depolarization in OFFαGCs, such as occurs during action potentials, may cause considerable depolarizing current flow into ACs (AC_{M2}) through the gap junctions. Because AC neurotransmitters are inhibitory, this reciprocal electrical synapse may serve as a negative feedback circuit for spiking activities in the OFFαGCs (Fig. 5).

In summary, the synaptic circuitry diagram (Fig. 5) derived from our study is primarily consistent with the general plan for ON and OFF ganglion cells set forth by anatomical studies, and thus our results provide the first physiological support for the organization found in the mouse retina. Additionally, our data elucidate which synapses serve physiological function and which ones do not, as well as which synapses are more dominant than others in mediating the light responses of the cells. For example, our data suggest that the primary function of the AC inputs to ONαGCs is to regulate the spiking frequency of the cells by voltage shunting and that the AII AC feedforward synapse is the dominant inputs for sOFFαGCs, at least within the low light intensity range. In addition, the outward ON ΔI_C and ON ΔI_{Cl} from HBC_{MC} and ACs to tOFFαGCs serve little physiological function, and the transient inward OFF ΔI_C from HBC_{SC}s is the

dominant input for the tOFFαGCs spike response. Finally, OFFαGCs, rather than ONαGCs, are likely to make functional reciprocal electrical synapses with ACs. These physiological characteristics of αGCs could not be revealed by the previous anatomical studies, and thus they provide new insights on our understanding of the functional circuitry of the mammalian retina.

References

Applebury ML, Antoch MP, Baxter LC, Chun LL, Falk JD, Farhangfar F, Kage K, Krzystolik MG, Lyass LA, Robbins JT (2000) The murine cone photoreceptor: a single cone type expresses both S and M opsins with retinal spatial patterning. Neuron 27:513–523.

Baylor DA (1987) Photoreceptor signals and vision. Proctor lecture [review]. Invest Ophthal Vis Sci 28:34–49.

Berntson A, Taylor WR (2000) Response characteristics and receptive field widths of on-bipolar cells in the mouse retina. J Physiol (Lond) 524:879–889.

Bloomfield SA, Dacheux RF (2001) Rod vision: pathways and processing in the mammalian retina. Prog Retin Eye Res 20:351–384.

Bloomfield SA, Miller RF (1986) A functional organization of ON and OFF pathways in the rabbit retina. J Neurosci 6:1–13.

Bloomfield SA, Xin D (1997) A comparison of receptive-field and tracer-coupling size of amacrine and ganglion cells in the rabbit retina. Vis Neurosci 14:1153–1165.

Bolz J, Wassle H, Thier P (1984) Pharmacological modulation of on and off ganglion cells in the cat retina. Neuroscience 12:875–885.

Brandstatter JH, Koulen P, Wassle H (1998) Diversity of glutamate receptors in the mammalian retina. Vision Res 38:1385–1397.

Cleland BG, Levick WR, Wassle H (1975) Physiological identification of a morphological class of cat retinal ganglion cells. J Physiol (Lond) 248:151–171.

Cohen ED, Miller RF (1994) The role of NMDA and non-NMDA excitatory amino acid receptors in the functional organization of primate retinal ganglion cells. Vis Neurosci 11:317–332.

Cohen ED, Zhou ZJ, Fain GL (1994) Ligand-gated currents of alpha and beta ganglion cells in the cat retinal slice. J Neurophysiol 72:1260–1269.

Crooks J, Kolb H (1992) Localization of GABA, glycine, glutamate and tyrosine hydroxylase in the human retina. J Comp Neurol 315:287–302.

Dacey DM, Brace S (1992) A coupled network for parasol but not midget ganglion cells in the primate retina. Vis Neurosci 9:279–290.

Deans MR, Volgyi B, Goodenough DA, Bloomfield SA, Paul DL (2002) Connexin36 is essential for transmission of rod-mediated visual signals in the mammalian retina. Neuron 36:703–712.

Demb JB, Pugh EN (2002) Connexin36 forms synapses essential for night vision. Neuron 36:551–553.

DeVries SH, Baylor DA (1995) An alternative pathway for signal flow from rod photoreceptors to ganglion cells in mammalian retina. Proc Natl Acad Sci USA 92:10658–10662.

Doi M, Uji Y, Yamamura H (1995) Morphological classification of retinal ganglion cells in mice. J Comp Neurol 356:368–386.

Field GD, Rieke F (2002) Nonlinear signal transfer from mouse rods to bipolar cells and implications for visual sensitivity. Neuron 34:773–785.

Freed MA, Sterling P (1988) The ON-alpha ganglion cell of the cat retina and its presynaptic cell types. J Neurosci 8:2303–2320.

Howes KA, Pennesi ME, Sokal I, Church-Kopish J, Schmidt B, Margolis D, Frederick JM, Rieke F, Palczewski K, Wu SM, Detwiler PB, Baehr W (2002) GCAP1 rescues rod photoreceptor response in GCAP1/GCAP2 knockout mice. EMBO J 21:1545–1554.

Hubel DH, Wiesel TN (1968) Receptive fields and functional architecture of monkey striate cortex. J Physiol (Lond) 195:215–243.

Jacoby R, Stafford D, Kouyama N, Marshak D (1996) Synaptic inputs to ON parasol ganglion cells in the primate retina. J Neurosci 16:8041–8056.

Jeon CJ, Strettoi E, Masland RH (1998) The major cell populations of the mouse retina. J Neurosci 18:8936–8946.

Kolb H, Famiglietti EV (1974) Rod and cone pathways in the inner plexiform layer of cat retina. Science 186:47–49.

Kolb H, Nelson R (1981) Amacrine cells of the cat retina. Vision Res 21:1625–1633.

Kolb H, Nelson R (1983) Rod pathways in the retina of the cat. Vision Res 23:301–312.

Kuffler SW (1953) Discharge patterns and functional organization of the mammalian retina. J Neurophysiol 16:37–68.

Lyubarsky AL, Falsini B, Pennesi ME, Valentini P, Pugh EN Jr (1999) UV- and midwave-sensitive cone-driven retinal responses of the mouse: a possible phenotype for coexpression of cone photopigments. J Neurosci 19:442–455.

Meister M, Wong RO, Baylor DA, Shatz CJ (1991) Synchronous bursts of action potentials in ganglion cells of the developing mammalian retina. Science 252:939–943.

Nelson R, Famiglietti Jr EV, Kolb H (1978) Intracellular staining reveals different levels of stratification for on- and off-center ganglion cells in cat retina. J Neurophysiol 41:472–483.

Nelson R, Kolb H, Robinson MM, Mariani AP (1981) Neural circuitry of the cat retina: cone pathways to ganglion cells. Vision Res 21:1527–1536.

Pang JJ, Gao F, Wu SM (2002) Relative contributions of bipolar cell and amacrine cell inputs to light responses on ON, OFF and ON–OFF retinal ganglion cells. Vision Res 42:19–27.

Peichl L (1989) Alpha and delta ganglion cells in the rat retina. J Comp Neurol 286:120–139.

Peichl L, Wassle H (1981) Morphological identification of on- and off-centre brisk transient (Y) cells in the cat retina. Proc R Soc Lond B Biol Sci 212:139–153.

Pourcho RG, Owczarzak MT (1989) Distribution of GABA immunoreactivity in the cat retina: a light- and electron-microscopic study. Vis Neurosci 2:425–435.

Pourcho RG, Owczarzak MT (1991) Connectivity of glycine immunoreactive amacrine cells in the cat retina. J Comp Neurol 307:549–561.

Qin P, Pourcho RG (1996) Distribution of AMPA-selective glutamate receptor subunits in the cat retina. Brain Res 710:303–307.

Saito HA (1983) Morphology of physiologically identified X-, Y-, and W-type retinal ganglion cells of the cat. J Comp Neurol 221:279–288.

Schneeweis DM, Schnapf JL (1995) Photovoltage of rods and cones in the macaque retina. Science 268:1053–1056.

Soucy E, Wang Y, Nirenberg S, Nathans J, Meister M (1998) A novel signaling pathway from rod photoreceptors to ganglion cells in mammalian retina. Neuron 21:481–493.

Sun W, Li N, He S (2002) Large-scale morphological survey of mouse retinal ganglion cells. J Comp Neurol 451:115–126.

Thibos LN, Werblin FS (1978) The response properties of the steady antagonistic surround in the mudpuppy retina. J Physiol (Lond) 278:79–99.

Tian N, Hwang TN, Copenhagen DR (1998) Analysis of excitatory and inhibitory spontaneous synaptic activity in mouse retinal ganglion cells. J Neurophysiol 80:1327–1340.

Tsukamoto Y, Morigiwa K, Ueda M, Sterling P (2001) Microcircuits for night vision in mouse retina. J Neurosci 21:8616–8623.

Vardi N, Masarachia PJ, Sterling P (1989) Structure of the starburst amacrine network in the cat retina and its association with alpha ganglion cells. J Comp Neurol 288:601–611.

Wassle H, Boycott BB (1991) Functional architecture of the mammalian retina [review]. Physiol Rev 71:447–480.

Werblin FS (1978) Transmission along and between rods in the tiger salamander retina. J Physiol (Lond) 280:449–470.

Williams RW, Strom RC, Rice DS, Goldowitz D (1996) Genetic and environmental control of variation in retinal ganglion cell number in mice. J Neurosci 16:7193–7205.

Wu SM (1987) Synaptic connections between neurons in living slices of the larval tiger salamander retina. J Neurosci Methods 20:139–149.

Wu SM, Gao F, Maple BR (2000) Functional architecture of synapses in the inner retina: segregation of visual signals by stratification of bipolar cell axon terminals. J Neurosci 20:4462–4470.

Xin D, Bloomfield S (1997) Tracer coupling pattern of amacrine and ganglion cells in the rabbit retina. J Comp Neurol 383:512–528.